Singular-point characterization in microscopic flows

Giorgio Volpe,[1] Giovanni Volpe,[1] and Dmitri Petrov[1,2]
[1]*Institut de Ciencies Fotoniques (ICFO), Mediterranean Technology Park, 08860, Castelldefels (Barcelona), Spain*
[2]*Institució Catalana de Recerca i Estudis Avançats (ICREA), 08010, Barcelona, Spain*
(Received 3 August 2007; revised manuscript received 20 December 2007; published 11 March 2008)

We suggest an approach to microrheology based on optical traps capable of measuring fluid fluxes around singular points of fluid flows. We experimentally demonstrate this technique, applying it to the characterization of controlled flows produced by a set of birefringent spheres spinning due to the transfer of light angular momentum. Unlike the previous techniques, this method is able to distinguish between a singular point in a complex flow and the absence of flow at all; furthermore it permits us to characterize the stability of the singular point.

DOI: 10.1103/PhysRevE.77.037301 PACS number(s): 47.61.−k, 05.40.Jc, 47.60.−i, 87.80.Cc

The experimental characterization of fluid flows in microenvironments is important both from a fundamental point of view and from an applied one, since for many applications it is required to assess the performance of microfluidic structures, such as lab-on-a-chip devices [1]. Carrying out this kind of measurements can be extremely challenging. In particular, due to the small size of these environments, wall effects cannot be neglected [2]. Additional difficulties arise studying biological fluids because of their complex rheological properties.

In the cases of practical interest the flow is strongly viscous (creeping motions or Stokes flows) and a low Reynolds number regime can be assumed [3]. Since the creeping motion regime is a particular case of a laminar regime, it is possible to univocally define a time-independent pressure and velocity field. Therefore, a well-defined drag force field acts on a particle immersed in the fluid flow. Ideally microflow sensors should be able to monitor the streamlines in real time and in the least invasive way. One common method to achieve this goal is to measure the drag force field acting on a probe particle, resorting to statistical criteria of analysis because of the intrinsic presence of Brownian motion.

Recently optically trapped microscopic particles have been proposed as flow sensors [4–8]. An optical trap enables the confinement of micron sized objects [9]. In [4] an oscillating optically trapped probe is used to map the two-dimensional flow past a microscopic wedge. In [5,6] a stress microviscometer is presented: it generates and measures microscopic fluid velocity fields, monitoring the probe particle displacement. A further improvement was achieved in Ref. [8] by using multiple holographic optical traps in order to parallelize the technique: an array of microprobes can be simultaneously trapped and used to map out the streamlines. All these techniques apply a photonic force microscope (PFM) approach [10–14] to the flow measurement: the fluid velocity at the trap location is obtained by monitoring the probe displacements resulting from the balance between the trapping and drag forces.

The techniques described above present a major drawback: they interpret the experimental results assuming that the flow can be described by a set of parallel streamlines. Then the drag force acting on a probe around a specific point in the flow is well described by a constant value, and this is the case considered by the current optical trap methods. However, the drag force field may include singular points as well. In these points the flow and, hence, the drag force are null, but not in its surrounding. The question, which arises naturally, is how to characterize this flow. Under the assumption of a steady incompressible flow, a zero body force, and low Reynolds numbers, the local fluid motion satisfies the quasistatic Stokes equations [3]: $\eta\nabla^2\mathbf{v}=\nabla p$, $\nabla\cdot\mathbf{v}=0$, where $\mathbf{v}$ is the velocity, p the pressure, and η the dynamic viscosity. Since the fluid is incompressible and there are no sources or sinks, there can be only two kinds of singular points [15]: (1) saddles (unstable) at the meeting point between two opposite flowing streamlines or (2) centra (stable) in presence of a nonzero curl. As we show below, the characterization of the flow near these points can be achieved by studying the statistical properties of the Brownian motion of the probe.

The knowledge of the flow-field near a singular point is of relevance for fundamental physical studies as well as for engineering applications. The mixing of fluids flowing through microchannels is important for many chemical application; a reduction of the mixing length can be achieved by the generation of a transverse flow [16], in which case the formation of singular points is inevitable. In biological systems creeping motions take place in small blood or linfatic vessels or at the interface between tissues and prothesis or artificial organs [17]. In the presence of slow flows, macrophage adhesion becomes more probable, increasing the possibilities of inflammation. Furthermore, the growth rate of thrombi, due to platelet aggregation, is also determined by the characteristics of the flow around it: for example, the presence of stable equilibrium points, such as centra, helps their formation and growth [18]. Flow measurements at the microscale can help to diagnose pathologies and to guide the design of biomaterials and nanodevices for diagnostic or therapeutic goals.

In this paper we extend the PFM-approach to microrheology in order to characterize fluid fluxes in the proximity of singular points. The concept is to monitor the position of an optically trapped probe in order to locally characterize the drag force field as a generic function of the space coordinates up to the first order in its Taylor expansion around the probe position. The full theoretical description of the corresponding stochastic equations will be published elsewhere [19]. This technique permits us to distinguish between a singular point in a complex flow and the absence of flow at all. Further-

more our approach allows one to determine the stability of these singular points, which can be relevant for applications.

In the following we consider the drag force field produced by a bidimensional laminar regime. Since in microfluidic and lab-on-a-chip devices a planar geometry is generally assumed, this is the most useful case for applications. Nevertheless, if needed, our approach can be generalized to the three-dimensional case.

We generated three kinds of fluid flow—namely, a set of parallel streamlines, a saddle or a centrum—using solid spheres made of a birefringent material [5] [calcium vaterite crystals (CVC), radius $R=1.5\pm0.2$ μm], which rotate due to the transfer of spin angular momentum of light. They are all optically controlled, i.e., their positions are controlled by optical traps and their spinning state is controlled through the polarization state of the light. The angular velocity of the CVC sphere is given by $\omega=\Delta\sigma\lambda P/16\pi^2\eta R^3 c$, where $\Delta\sigma$ is the change of the light spin momentum due to the scattering on the probe, P the beam power, η the medium viscosity, c the speed of light, and λ the wavelength of the optical field. In the experimental realization up to four CVC spheres were optically trapped in water and put into rotation using four steerable 1064 nm beams from a Nd:YAG laser with controllable polarization—to control the direction of the rotation—and power—to control the rotation rate. A probe polystyrene sphere (radius $r=500$ nm) was held by an optical trap produced by a 632 nm linearly polarized beam. The stiffness of this trap was adjustable through the power. The forward scattered light of this latter beam served to track the probe position using a position sensor based on a quadrant-photodetector (QPD). The presence of these particle close to each other can have an influence on their Brownian motion; however, these are second-order effects that can be neglected in our approximation (see, for example, Ref. [20]).

Assuming no slip at the particle surface, the quasi-Stokes equation leads to the following solution for the flow velocity near a single spinning sphere [3,6]:

$$\mathbf{v}=\omega\mathbf{e}_z\times\mathbf{x}\frac{R^3}{\|\mathbf{x}\|^3}. \tag{1}$$

In each point in the proximity of the rotating sphere the streamlines are perpendicular to the plane containing the z axis (unit vector $\mathbf{e}_z$) and the coordinate vector $\mathbf{x}$.

In Fig. 1 the results for probing such a drag force field near a single spinning sphere ($\omega\approx38$ rad/s) are presented. The induced drag force was measured through the shift of the equilibrium position of the probe [Figs. 1(b), 1(d), and 1(f)] and after calibrating the stiffness of the probe trap ($k=175\pm15$ fN/μm). The corresponding force field can be reconstructed [Figs. 1(c) and 1(e)]: the forces acting on the probe particle result 40 ± 5 fN (counterclockwise rotation) and 37 ± 5 fN (clockwise rotation). These results are in agreement with the force that is expected to act on the probe sphere in the presence of a flow velocity given by Eq. (1) [5,6]. In all figures, except Fig. 4, for each plot data acquired during 150 s with sampling rate 2000 Hz were analyzed.

In a system with n spinning spheres, the linearity of the quasi-Stokes equations [3] allows one to use the superposition of solutions (1) in order to obtain the total flow. Since the velocity in the equatorial plane is proportional to the reciprocal square of the distance from the sphere center, the flow velocity vanishes at a distance of a few sphere radii. Hence, in first approximation the hydrodynamic interaction between the spinning spheres located far enough from each other can be neglected. For $n=2$ or $n=4$ we assume the spheres to be symmetrically displaced at the same distance ρ with respect to the origin $\mathbf{x}_0$ [Figs. 3(a) and 4(a)], so that the origin is a singular point, i.e., $\mathbf{v}(\mathbf{x}_0)=0$. The velocity field can be locally approximated as

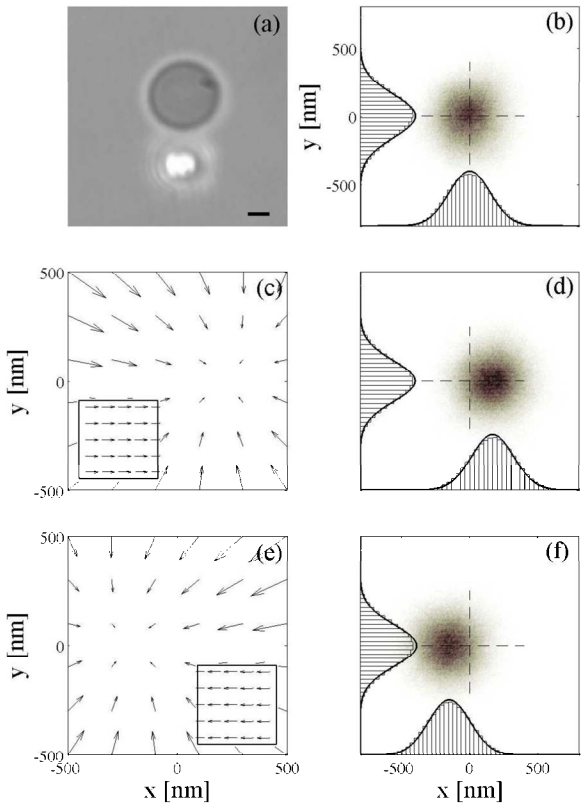

FIG. 1. (Color online) (a) Image of a trapped probe near a single spinning sphere. The bar is 1 μm. (b) 2D probability density function (PDF) when the spinning sphere is at rest. (c)–(f) Experimental probability density functions and reconstructed total force field. Insets: reconstructed hydrodynamic force field near $x=0$ and $y=0$. The reconstruction is accurate only over the region visited by the Brownian particle. The sphere is spinning (c)–(d) counterclockwise and (e)–(f) clockwise.

$$\mathbf{v}=\omega R^3\mathbf{J}\cdot\mathbf{x}=\omega R^3\sum_{i=1}^{n}\mathbf{J}_i\cdot\mathbf{x}, \tag{2}$$

where $\omega R^3\mathbf{J}$ is the Jacobian matrix of the total velocity field evaluated in the singular point and $\omega R^3\mathbf{J}_i$ the Jacobian matrix of the velocity field generated by particle i evaluated in the same point. Since the prefactor ωR^3 is positive and constant, in the stability analysis we can consider only $\mathbf{J}$. As expected, since the fluid is incompressible, Tr($\mathbf{J}$) is always null. This means that only (unstable) saddles—with

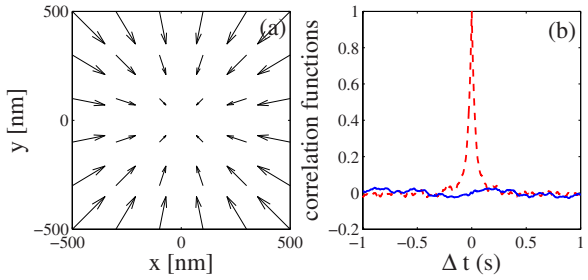

FIG. 2. (Color online) (a) Force field and (b) autocorrelation (red dashed line) and cross-correlation (blue solid line) functions when only the optical force is acting on a 0.5 μm radius probe in absence of drag force field.

$n=2$, $\det(\mathbf{J})=-4/\rho<0$—or (stable) centra—with $n=4$, $\det(\mathbf{J})=2/\rho>0$—can exist.

In Figs. 2–4 the experimental results for such cases are presented. We followed the data analysis procedure detailed in Ref. [19]. Briefly, the total force field acting on the probe is given by the sum of the drag force-field and the restoring force due to the harmonic trapping potential. The drag force field can be decomposed into a conservative and a rotational part, while the optical force field is purely conservative. Our aim is to separate these three contributions. The rotational component of the drag force field can be obtained from the difference of the cross-correlation functions [19,21]

$$D_{\mathrm{CCF}}(\Delta t) = \langle x(t)y(t+\Delta t)\rangle - \langle y(t)x(t+\Delta t)\rangle, \qquad (3)$$

which vanishes only if the rotational part of the drag force field is null. If D_{CCF} does not vanish, i.e., in the presence of a centrum, the rotational component of the drag force field can be calculated from its slope around $\Delta t=0$.

If the rotational component, and therefore D_{CCF}, is null, the total force field is purely conservative, and the conservative component of the drag force field can be calculated by subtracting the optical potential from the total potential, derived from the 2D probability density function (PDF) of the probe position. This can only be done if the total force field is conservative and, therefore, a first step is to verify that D_{CCF} vanishes. Some results for an optically trapped probe in the absence of flow are presented in Fig. 2: the optical force-field is harmonic [Fig. 2(a)] and it is purely conservative [its D_{CCF} is null, Fig. 2(b)].

In Fig. 3 the flow is generated by two CVCs ($\omega \approx 38$ rad/s), symmetrically positioned with respect to the

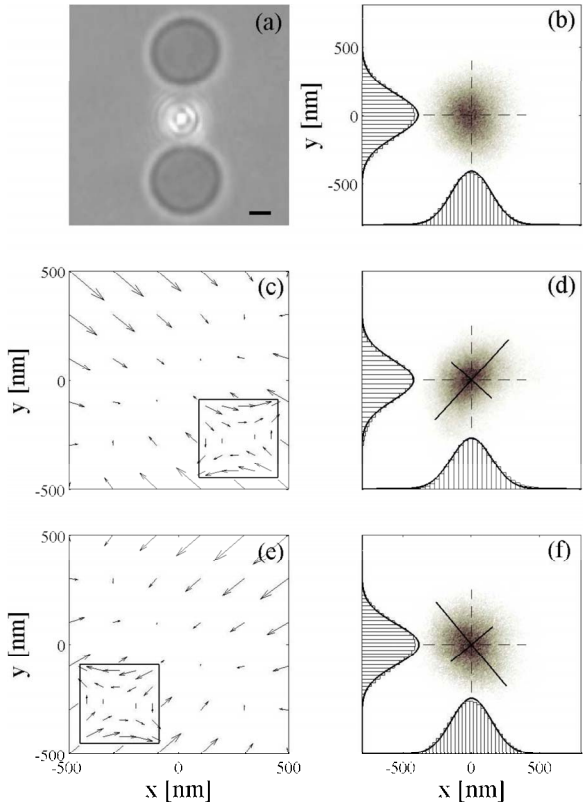

FIG. 3. (Color online) (a) Image of a trapped probe between a couple of spinning spheres. The bar is 1 μm. (b) 2D probability density function (PDF) when the spinning spheres are at rest. (c)–(f) Experimental probability density functions and reconstructed total force field. Insets: reconstructed hydrodynamic force field near $x=0$ and $y=0$. The reconstruction is accurate only over the region visited by the Brownian particle. The spheres are spinning (c),(d) counterclockwise and (e),(f) clockwise.

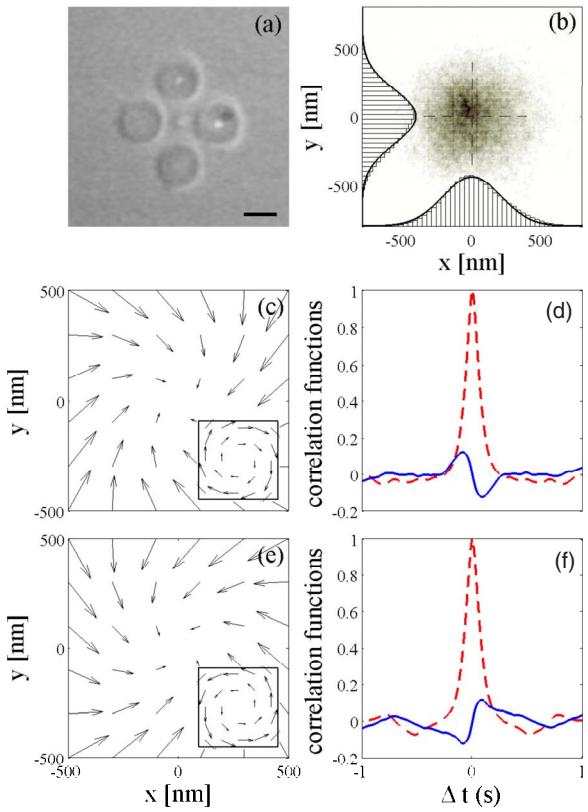

FIG. 4. (Color online) (a) Image of a trapped probe between four spinning spheres. The bar is 3 μm. (b) 2D probability density function when the spinning sphere is at rest. (c)–(f) Total force fields—insets: drag force field contribution—and autocorrelation (red dashed line) and cross-correlation (blue solid line) functions when the sphere is spinning (c),(d) counterclockwise and (e),(f) clockwise. For each of the plots (b), (d), and (e) ten data sets acquired during 15 s with sampling rate 2000 Hz were analyzed and averaged.

probe [Fig. 3(a)]. The position of the probe is chosen so that there is no shift in the equilibrium position regardless of the rotation state of the spheres [Figs. 3(b), 3(d), and 3(f)]. Since within the experimental error the experimental D_{CCF} is found to be null, we conclude that the rotational component of the drag force field is negligible and we reconstruct its conservative part by subtracting the optical restoring force-field from the total force field [Figs. 3(c) and 3(e)]. The optical trap produces a symmetric harmonic potential ($k=185\pm20$ fN/μm) [Fig. 3(b)]. With spinning spheres the PDF becomes ellipsoidal [Figs. 3(d) and 3(f)]. For the spheres rotating counterclockwise [Figs. 3(c) and 3(d)], the major axis of the PDF ellipse is oriented at 40°, the stiffness is $k_{min}=142\pm20$ fN/μm along the major axis and $k_{max}=261\pm20$ fN/μm along the minor axis. For a clockwise rotation [Figs. 3(e) and 3(f)], the major axis is oriented at 42°, the stiffness is $k_{min}=165\pm20$ fN/μm along the major axis and $k_{max}=211\pm20$ fN/μm along the minor axis (the rotation rate was observed to be different in the two directions). These results are in good agreement with what is expected from a flow velocity (2). The data agree well with a Gaussian PDF so that the flow acts as a perturbation on the Brownian motion of the probe. The corresponding total force fields are represented in Figs. 3(c) and 3(e), while the drag force field contributions are depicted in the insets: they constitute, indeed, saddle points.

In Fig. 4 the characterization of a fluid flow near a singular point of the second kind, a centrum, is presented. This stable singular point was generated by four CVC spheres ($\omega\approx38$ rad/s) symmetrically distributed with respect to the probe [Fig. 4(a)] in an optical trap with stiffness $k=78\pm5$ fN/μm. We observed that the PDFs of the probe position do not depend on the rotation direction of the spinning spheres [Fig. 4(b)]. However, D_{CCF} is not null [Figs. 4(d) and 4(f)], showing the presence of a rotational component of the drag force field. This component produces a torque on the probe and the probe rotates with a constant angular velocity Ω, whose value results from a balance between the torque applied to the probe and the drag torque [21]. $\gamma\Omega\langle x^2+y^2\rangle=5.7\pm1.3$ fN μm for the spheres rotating counterclockwise [Figs. 4(c) and 4(d)] and 6.4 ± 1.3 fN μm for the spheres rotating clockwise [Figs. 4(e) and 4(f)], where $\langle x^2+y^2\rangle$ is the mean square displacement of the probe. These results are in good agreement with what is expected from a flow velocity given by Eq. (2). The resulting total and drag force fields are represented in Figs. 4(c) and 4(e), while the drag force field contributions are depicted in the insets: they constitute, indeed, a centrum. However, the size of the probe particle is only 4.5 times smaller that the size of the flux so that the probe can provide perturbations in the distribution of the flux.

In conclusion, we have demonstrated the use of an optically trapped probe for the characterization of singular points in microscopic flows. This technique delivers previously inaccessible information that can be exploited for a higher understanding and optimization of microfluidic flows in the presence of singular points. A method that makes profit of the reconfigurable holographic optical tweezers, and that uses single tracer particles to measure the velocity field has been already proposed [8]. It requires monitoring the positions of several particles. We propose to collect the same information using fewer particles—just one: the probe itself in its Brownian motion visits the region around the singular point acquiring information about the flows. In this case one needs to measure the position of one particle that can be done more easily, for instance, by a quadrant photodetector. In comparison with previously available techniques, the method we propose makes a more profitable use of the information provided the Brownian motion of the particle. The further study of the accuracy of the method and its direct comparison with other methods is, of course, a next step.

The authors acknowledge useful discussions with N. Heckenberg, A. Bagno, and M. Rubí. This research was carried out with the financial support of the Spanish Ministry of Education and Science. It was also partially supported by the Departament d'Universitats, Recerca i Societat de la Informació and the European Social Fund.

[1] J. Knight, Nature (London) **418**, 474 (2002).
[2] Y. Zhu and S. Granick, Phys. Rev. Lett. **87**, 096105 (2001).
[3] J. Happel and H. Brenner, *Low Reynolds Number Hydrodynamics* (Spinger, New York, 1983).
[4] B. A. Nemet and M. Cronin-Golomb, Opt. Lett. **27**, 1357 (2002).
[5] A. I. Bishop, T. A. Nieminen, N. R. Heckenberg, and H. Rubinsztein-Dunlop, Phys. Rev. Lett. **92**, 198104 (2004).
[6] G. Knöner, S. Parkin, N. R. Heckenberg, and H. Rubinsztein-Dunlop, Phys. Rev. E **72**, 031507 (2005).
[7] G. Pesce, A. Sasso, and S. Fusco, Rev. Sci. Instrum. **76**, 115105 (2005).
[8] R. Di Leonardo, J. Leach, H. Mushfique, J. M. Cooper, G. Ruocco, and M. J. Padgett, Phys. Rev. Lett. **96**, 134502 (2006).
[9] K. C. Neuman and S. M. Block, Rev. Sci. Instrum. **75**, 2787 (2004).
[10] L. Ghislain and W. W. Webb, Opt. Lett. **18**, 1678 (1993).
[11] J. H. E. Florin, A. Pralle, and E. Stelzer, J. Struct. Biol. **119**, 202 (1997).
[12] A. Rohrbach and E. Stelzer, J. Appl. Phys. **91**, 5474 (2002).
[13] K. Berg-Sørensen and H. Flyvbjerg, Rev. Sci. Instrum. **75**, 594 (2004).
[14] G. Volpe, G. Kozyreff, and D. Petrov, J. Appl. Phys. **102**, 084701 (2007).
[15] M. W. Hirsch, S. Smale, and R. Devaney, *Differential Equations, Dynamical Systems, and an Introduction to Chaos* (Academic Press, San Diego, 2006).
[16] A. D. Stroock, S. K. W. Dertinger, A. Ajdari, I. Mezić, H. A. Stone, and G. W. Whitesides, Science **295**, 647 (2002).
[17] A. Belanger, *Vascular Anatomy and Physiology: An Introductory Text* (Davies, Pasadena, 1990).
[18] M. F. Modest and H. Zhang, ASME J. Heat Transfer **124**, 30 (2002).
[19] G. Volpe, G. Volpe, and D. Petrov, Phys. Rev. E **76**, 061118 (2007).
[20] M. Reichert and H. Stark, Phys. Rev. E **69**, 031407 (2004).
[21] G. Volpe and D. Petrov, Phys. Rev. Lett. **97**, 210603 (2006).